A Theoretical Basis for Extending Surface-Paneling Methods to Transonic Flow

Larry L. Erickson* and Shawn M. Strande*
NASA Ames Research Center, Moffett Field, California

The surface integral terms in Green's third identity are often used to solve the Prandtl-Glauert (linear potential-flow) equation with panel methods. This can be done, as in the PAN AIR code, for either subsonic or supersonic flow about complete aircraft. The extension to transonic flow is suggested by the volume integral term of Green's third identity. The mathematical basis for this extension, without the use of body-fitted grids, is presented. Supercritical transonic results computed from a two-dimensional transonic PAN AIR research code demonstrate the method.

Nomencalture

M_∞ = freestream Mach number
$\hat{n},n$ = unit normal, iteration counter
$\vec{v}$ = (u,v,w), perturbation velocity, $\vec{\nabla}\phi$
$\vec{V}_\infty$ = freestream velocity
α = angle of attack
$\delta(\ )$ = change (variation) in ( )
$\Delta[\ ]$ = jump in [ ]
μ = doublet strength
ρ = fluid density
σ = source strength
ϕ = perturbation potential
$\vec{\nabla}$ = gradient operator
$\tilde{\nabla}^2$ = $\vec{\nabla}\cdot\vec{\nabla}$
$\{\ \}$ = column matrix
$\cdot$ = vector dot product

Subscripts

i,j = control-point or grid-point index
P = arbitrary point, usually taken to be a control point or grid point
x,y,z = differentiation with respect to x, y, and z

I. Introduction

ALTHOUGH a great deal of progress has been made in solving nonlinear fluid flow problems by finite difference methods, these methods have not yet proved to be easily adaptable to complex three-dimensional surfaces. According to Ref. 1 the major technical obstacle to computing inviscid transonic flow about complete aircraft "is the difficulty in generating 'suitable' grids."

The finite element method, another numerical approach to solving partial differential equations, is easily adaptable to arbitrary geometry in solid mechanics problems. The finite element method also appears to offer promise for nonlinear fluid mechanics problems.[2]

The best-developed and most widely used methods for computing flow about arbitrary geometries are those which represent the configuration boundary with some form of source/doublet-vorticity distributions, generally called surface panels. Historically, panel methods have been limited to solving problems governed by the linear Prandtl-Glauert equation. Recent studies[3-6] have shown that surface panels used in conjunction with field grids can also solve nonlinear problems. The approach of Ref. 6 combines PAN AIR[7-10] linear-source, quadratic-doublet panels with a rectangular grid of points (in physical space) that is independent of the surface geometry. Thus, the entire problem of creating a surface-conforming grid is avoided. The surface geometry and boundary conditions are defined by, and imposed with, panels. Consequently, PAN AIR models would change from panels alone to panels plus a rectangular grid (Fig. 1). The rectangular grid is not used for the conventional purpose of replacing the governing partial differential equation(s) with finite difference approximations; rather, it is used to evaluate certain volume integrals with fast Fourier transforms.

Since panel methods are usually considered to be superposition methods, their extension to nonlinear problems may seem surprising. The theoretical basis for this extension can be shown using Green's third identity, as shown in Sec. II. The related, but more powerful, mathematical approach of Ref. 6 is discussed in Sec. III. Numerical results for two-dimensional supercritical flow about NACA 0012 and circular-arc airfoils are presented in Sec. IV.

II. Green's Third Identity as a Means to Extend Panel Methods to Nonlinear Potential Flow

The full-potential equation can be written as [see Ref. 11, Eq. (7)]

$$\vec{\nabla}\cdot(\rho\vec{V}) = 0 \tag{1a}$$

where

$$\vec{V} = \vec{V}_\infty + \vec{\nabla}\phi, \qquad \rho = \rho(\vec{V}) \tag{1b}$$

The full-potential equation can also be written as [see Ref. 12, Eq. (8.5)]

$$(1-M_\infty^2)\phi_{xx} + \phi_{yy} + \phi_{zz} = M_\infty^2\left[(\gamma+1)\phi_x + \left(\frac{\gamma+1}{2}\right)\phi_x^2 + \left(\frac{\gamma-1}{2}\right)(\phi_y^2+\phi_z^2)\right]\phi_{xx} + \ldots \tag{2a}$$

where the left-hand side of Eq. (2a) contains only linear terms, and the right-hand side contains only nonlinear terms. For convenience, we introduce some shorthand notation to write Eq. (2a) as

$$\tilde{\nabla}^2\phi = G(\phi_x, \phi_x^2, \ldots) \tag{2b}$$

which can be thought of as a Poisson equation with a nonlinear right-hand side. If the product of M_∞^2 and the

Presented as Paper 83-1831 at the AIAA Applied Aerodynamics Conference, Danvers, MA, July 13-15, 1983; received April 11, 1984; revision received March 4, 1985. This paper is declared a work of the U.S. Government and therefore is in the public domain.

*Research Scientist. Member AIAA.

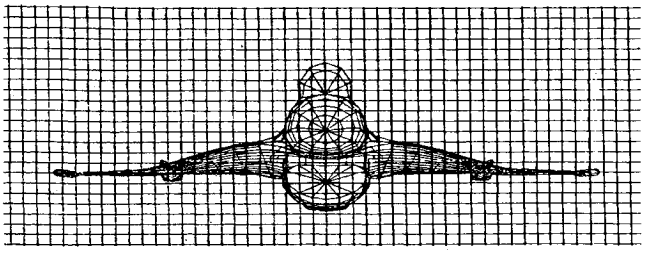

Fig. 1 Panels plus rectangular grid.

nonlinear terms are neglected, Eqs. (2) reduce to the Prandtl-Glauert equation

$$\tilde{\nabla}^2\phi = 0 \tag{3}$$

Boundary-value problems governed by Eq. (3) are currently solved by PAN AIR. This is done by computing influence coefficients for ϕ (and for $\vec{v} = \vec{\nabla}_P\phi$) from the following equation [see Ref. 9, Eq. (B.0.1)]:

$$\phi(P) = \iint_S (\sigma K_\sigma + \mu K_\mu)\,dS \tag{4}$$

and then imposing boundary conditions on S. The symbols in Eq. (4) are defined as

$$K_\sigma = \frac{-1}{k} \times \frac{1}{r}, \qquad K_\mu = \frac{1}{k}\hat{n}\cdot\tilde{\nabla}_Q\left(\frac{1}{r}\right)$$

$$r^2 = (x_Q - x_P)^2 + \beta^2(y_Q - y_P)^2 + \beta^2(z_Q - z_P)^2$$

$$\beta^2 = 1 - M_\infty^2, \qquad \sigma = \Delta(\hat{n}\cdot\vec{w}), \qquad \mu = \Delta\phi$$

$$\vec{w} = (\beta^2 u, v, w) = (\beta^2\phi_x, \phi_y, \phi_z) \tag{5}$$

The subscript Q denotes a variable point of surface S; the subscript P denotes a fixed point in the flowfield, or of S. For $M_\infty < 1$, $k = 4*\pi$ and S is the entire surface of the aircraft. For $M_\infty > 1$, $k = 2*\pi$ and S is that portion of the aircraft surface that lies in the upstream Mach cone emanating from point P.

Green's Third Identity

Equation (4) is often interpreted as a superposition of the potentials due to the source $(1/r)$ and doublet $[\hat{n}\cdot\tilde{\nabla}(1/r)]$ solutions of Eq. (3). Perhaps more fundamentally, Eq. (4) is a construction that forces ϕ to satisfy Eq. (3). This can be demonstrated by first considering Green's third identity [see Ref. 13, p. 221, Eq. (7)], and then relating it to potential-flow problems. Green's third identity is

$$\psi_P \equiv \iint_S [\Delta(\hat{n}\cdot\vec{\nabla}\psi)\times K_\sigma + \Delta\psi \times K_\mu]\,dS + \iiint_R \nabla^2\psi \times K_\sigma\,dR \tag{6}$$

The above identity relates the values of an arbitrary scalar function ψ, and its first and second derivatives, in domain (volume) R to the value of ψ at a particular point P, and to the jump in ψ and the jump in normal derivative of ψ across the surface(s) S that bound R. [The other quantities in identity equation (6) are the same as in Eq. (5) if M_∞ is set to zero there.] This identity is not a statement of any fluid mechanics laws, but it can be used to solve linear or nonlinear potential-flow problems. If ψ and $\vec{\nabla}\psi$ are continuous everywhere, the surface integrals in Eq. (6) vanish and the volume integral then becomes an integrating formula for Poisson's equation, $\nabla^2\psi = p(x,y,z)$. This property will be used in Eq. (39) as a key step in the transonic PAN AIR algorithm.

To solve potential-flow problems, the scalar ψ in Eq. (6) is taken to be the perturbation velocity potential ϕ. The identity can then be used to solve incompressible potential-flow problems. For compressible flow, identity (6) can be generalized to the form

$$\phi_P \equiv \iint_S [\sigma K_\sigma + \mu K_\mu]\,dS + \iiint_R (\tilde{\nabla}^2\phi) K_\sigma\,dR \tag{7}$$

where the symbols have the same meaning as those in Eqs. (3) and (5). Equation (7) then, is essentially identity (6) expressed in more familiar terms. Equation (7) states that the velocity potential at a particular point P is computable from source and doublet surface distributions on S (taken to be the aircraft surface and wakes), and from the spatial distribution of $\tilde{\nabla}^2\phi$ in the volume bounded (wetted) by both sides of S. If ϕ is constructed according to Eq. (4), normally thought of as a superposition of source and doublet solutions, it follows from Eq. (7) that

$$\iiint_R (\tilde{\nabla}^2\phi) K_\sigma\,dR = 0 \tag{8}$$

Since K_σ is a function of the arbitrary fixed point P, Eq. (8) implies that Eq. (3), the Prandtl-Glauert equation, has been satisfied throughout R.

To solve the nonlinear full potential equation (1a), imagine that ϕ is not constructed according to Eq. (4) but instead is constructed according to

$$\phi_P = \iint_S [\sigma K_\sigma + \mu K_\mu]\,dS + \iiint_R \vec{\nabla}\cdot[\tilde{\nabla}\phi - \rho\vec{V}] K_\sigma\,dR \tag{9}$$

Because $\phi(x,y,z)$ appears in the integrand of the last term, $\phi(x_P, y_P, z_P)$ cannot be constructed directly as it was with Eq. (4). Thus, the distribution $\phi(x,y,z)$ that satisfies Eq. (9) and the boundary conditions on S must be determined by some iterative method. If this is done, it follows from Eq. (7) that

$$\iiint_R \vec{\nabla}\cdot(\rho\vec{V}) K_\sigma\,dR = 0 \tag{10}$$

which implies that Eq. (1a), the full-potential equation, has been satisifed throughout R.

Numerical Discretization

To solve the Prandtl-Glauert equation, PAN AIR computes ϕ_P according to Eq. (4). This is done by replacing the actual aircraft surface S with networks of contiguous, piecewise flat panels. On each panel, σ and μ are specified linear and continuous† quadratic functions, respectively, of a local panel-coordinate system. These functions contain unknown constants that are linearly related to so-called singularity parameters λ_i, which are unknown values of σ and μ at discrete control points of the panels. This allows the right-hand side of Eq. (4) to be integrated analytically, resulting in the discretized form

$$\phi_P = [IC]\{\lambda\} \tag{11}$$

† Discontinuous doublet distributions produce spurious line-vortex-type velocities that cause serious errors in supersonic flow.[7]

where [IC] is a row matrix of influence coefficients giving the potential at point P that is due to the source and doublet distributions of all of the panels (for unit values of λ_j).

The same surface-paneling process is used, but with an $L\times M\times N$ rectangular grid of points P_{gp} that encompasses and penetrates S, to solve the full-potential equation. The grid is shown in Fig. 1. The rectangular grid is used to evaluate numerically, the volume integral

$$f_P = \iiint_R \vec{\nabla}\cdot[\tilde{\nabla}\phi - \rho\vec{V}]K_o dR \tag{12}$$

associated with point P. (For the present we will assume this can be done. More will be said about this at the end of Sec. III.) Then a value ϕ_P at any point P, which may or may not be one of the grid points P_{gp}, could be constructed according to Eq. (9):

$$\phi_P = [IC]\{\lambda\} + f_P \tag{13}$$

This constructed value would be correct only if the set of values selected for $\phi(P_{gp})$ satisfies $\vec{\nabla}\cdot(\rho\vec{V})=0$ [see discussion of Eqs. (9) and (10)]. Thus, the construction given by Eq. (13) can be thought of as an iterative procedure whereby a guess for $\phi(P_{gp})$ at iteration n provides an updated value for ϕ_P,

$$\phi_P^{(n+1)} = [IC]\{\lambda\}^{(n)} + f_P^{(n)} \tag{14}$$

Solution Procedure

Equation (14) is used to construct systems of linear equations for two sets of points. The first set contains the panel control points, where boundary conditions are imposed. The second set contains the $L\times M\times N$ grid points used to evaluate Eq. (12). To be specific, assume there are 100 control points and 1000 grid points. In what follows, separate sets of equations will be established from Eq. (14). One set will be for the panel control points P_{cp} and the other set will be for the grid points P_{gp}.

For convenience, assume the boundary conditions are all of the form

$$\phi_{cp_j} = b_j, \qquad j=1,\ldots,100 \tag{15}$$

where b_j are specified values at the 100 control points. Then, for the nth guess for ϕ at the 1000 grid points, the values for f_{cp} at the 100 control points can be computed from Eq. (12), resulting in [from Eqs. (13) and (15)]

$$\underset{100\times 1}{\{\phi_{cp}\}} = \underset{100\times 100}{[AIC]}\ \underset{100\times 1}{\{\lambda\}^{(n)}} + \underset{100\times 1}{\{f_{cp}\}^{(n)}} = \underset{100\times 1}{\{b\}} \tag{16}$$

or

$$[AIC]\{\lambda\}^{(n)} = \{b\} - \{f_{cp}\}^{(n)} \tag{17}$$

where [AIC] is the (full) matrix of panel-to-panel aerodynamic influence coefficients, $\{b\}$ the right-hand side due to the boundary conditions, $-\{f_{cp}\}^{(n)}$ the right-hand side due to the volume integral, and $\{\lambda\}$ the set of unknown singularity parameters.

Repeating the above process for the grid points P_{gp} gives

$$\underset{1000\times 1}{\{\phi_{gp}\}^{(n+1)}} = \underset{1000\times 100}{[AIC]}\ \underset{100\times 1}{\{\lambda\}^{(n)}} + \underset{1000\times 1}{\{f_{gp}\}^{(n)}} \tag{18}$$

Equations (17) and (18) form the basis of the solution procedure, which is composed of the following steps.

1) Make an initial guess for $\overset{1000\times 1}{\{\phi_{gp}\}^{(1)}}$ so that $\overset{100\times 1}{\{f_{cp}\}^{(1)}}$ can be computed from Eq. (12). The simplest choice would be $\overset{1000\times 1}{\{\phi_{gp}\}^{(1)}}=\{0\}$, which would make $\overset{100\times 1}{\{f_{cp}\}^{(1)}}=\{0\}$; this choice corresponds to solving the linear Prandtl-Glauert equation. The singularity parameters can then be obtained from Eq. (17). Symbolically, we write

$$\{\lambda\}^{(1)} = [AIC]^{-1}\{b - f_{cp}^{(1)}\} \tag{19}$$

In actual practice $\{\lambda\}$ is obtained by a more efficient procedure of decomposing [AIC] into lower and upper triangular matrices, and performing forward and backward substitutions.

2) This is an intermediate step; the values $\{\lambda\}^{(1)}$ obtained in step 1 are used to update the potential only at grid points "near" the panels. (The reason for doing this will be explained later.) In the current example, imagine that 200 of the 1000 grid points are near the panels. Partitioning Eq. (18) according to whether the grid points are near or not near the panels gives

$$\underset{1000\times 1}{\{\phi_{gp}\}^{[1+\frac{1}{2}]}} = \begin{matrix}200\\800\end{matrix}\overset{1000\times 1}{\begin{Bmatrix}\phi_{gp}\\ \text{near}\\ \hline \phi_{gp}\\ \text{not}\\ \text{near}\end{Bmatrix}}{}^{[1+\frac{1}{2}]}$$

$$= \begin{matrix}200\\800\end{matrix}\overset{1000\times 100}{\begin{bmatrix}AIC_{near}\\ \hline 0\end{bmatrix}}\{\lambda\}^{(1)} + \begin{matrix}200\\800\end{matrix}\overset{100\times 1}{\begin{Bmatrix}f_{gp}\\ \text{near}\\ \hline f_{gp}\\ \text{not}\\ \text{near}\end{Bmatrix}}{}^{(1)} \tag{20}$$

$$\overset{200\times 1}{\begin{Bmatrix}\phi_{gp}\\ \text{near}\end{Bmatrix}}{}^{[1+\frac{1}{2}]} = \underset{200\times 100}{[AIC_{near}]}\ \underset{100\times 1}{\{\lambda\}^{(1)}} + \overset{200\times 1}{\begin{Bmatrix}f_{gp}\\ \text{near}\end{Bmatrix}}{}^{(1)}$$

usually set to zero for $n=1$ (21a)

$$\overset{800\times 1}{\begin{Bmatrix}\phi_{gp}\\ \text{not}\\ \text{near}\end{Bmatrix}}{}^{[1+\frac{1}{2}]} = \overset{800\times 1}{\begin{Bmatrix}f_{gp}\\ \text{not}\\ \text{near}\end{Bmatrix}}{}^{(1)}$$

usually set to zero for $n=1$ (21b)

The superscript $[1+\frac{1}{2}]$ denotes these are intermediate values for what will be $\overset{1000\times 1}{\{\phi_{gp}\}^{(2)}}$.

3) Substitute the step 2 intermediate values $\overset{1000\times 1}{\{\phi_{gp}\}^{[1+\frac{1}{2}]}}$ into Eq. (12). This produces updated values $\overset{1000\times 1}{\{f_{gp}\}^{[1+\frac{1}{2}]}}$ at all 1000 grid points, even if the initial guess for $\overset{1000\times 1}{\{\phi_{gp}\}^{(1)}}$ produces $\overset{1000\times 1}{\{f_{gp}\}^{(1)}}=\{0\}$.

4) Replace the $\overset{1000\times 1}{\{\phi_{gp}\}^{[1+\frac{1}{2}]}}$ values of step 2 with

$$\underset{1000\times 1}{\{\phi_{gp}\}^{(2)}} = \overset{1000\times 100}{\begin{bmatrix}AIC_{near}\\ \hline 0\end{bmatrix}}\ \underset{100\times 1}{\{\lambda\}^{(1)}} + \underset{1000\times 1}{\{f_{gp}\}^{[1+\frac{1}{2}]}} \tag{22}$$

(from step 2) (from step 3)

To obtain the next update, $\overset{1000\times 1}{\{\phi_{gp}\}^{(3)}}$, steps 1-4 are repeated, using iteration-2 values as new starting values in step 1. In step 1 we now need the nonzero values of $\overset{100\times 1}{\{f_{cp}\}^{(2)}}$, the effect of ϕ at all grid points on the 100 control points. These can be obtained by 1) computing $\overset{100\times 1}{\{f_{cp}\}^{(2)}}$ from Eq. (12), using $\overset{1000\times 1}{\{\phi_{gp}\}^{(2)}}$; or by the more efficient procedure of 2) using the $\overset{1000\times 1}{\{f_{gp}\}^{[1+\frac{1}{2}]}}$ values at grid points adjacent to the panels to find the control-point values by interpolation. [Even if the

integrand in Eq. (12) has a discontinuity across the panels, f_P does not. In fact, f_P and its first derivative are continuous (Ref. 13, p. 152).]

The process is then repeated until

$$\begin{aligned} {}^{1000\times 1}\{\phi_{gp}\}^{(n+1)} &\doteq {}^{1000\times 1}\{\phi_{gp}\}^{(n)} \\ {}^{100\times 1}\{\lambda\}^{(n+1)} &\doteq {}^{100\times 1}\{\lambda\}^{(n)} \end{aligned} \tag{23}$$

converges to a chosen degree of accuracy. (This condition will be met if the process is convergent; see the end of this section.)

Now let us see why steps 2-4 were used to obtain ${}^{1000\times 1}\{\phi_{gp}\}^{(2)}$ instead of computing the values from

$${}^{1000\times 1}\{\phi_{gp}\}^{(2)} = {}^{1000\times 100}[\mathrm{AIC}]_{gp}\,{}^{100\times 1}\{\lambda\}^{(1)} + {}^{100\times 1}\{f_{gp}\}^{(1)} \tag{24}$$

In Eq. (24), $[\mathrm{AIC}]_{gp}$ contains the influence coefficients for all grid points, not just grid points near the panels. Equation (24) is easier to understand than the step 2, 3, 4 sequence, but it also means that a much larger matrix of influence coefficients has to be computed and stored. For a practical three-dimensional case involving 10×10^6 grid points and 1×10^3 singularity parameters, 10×10^9 influence coefficients would have to be computed and stored. In contrast, the step 2, 3, 4 sequence requires only about 1×10^6 influence coefficients for the effects of the panels on each other (the square of the number of singularity parameters), plus another million or so influence coefficients for the effects of the panels on the "near" grid points. A decrease in the number of influence coefficients by three orders of magnitude or more makes the approach practical.

The error introduced by the step 2, 3, 4 sequence is proportional to the square of the distance between grid points.[17] For the 65×65 grid described in Sec. IV, the approximate step 2, 3, 4 sequence gives essentially the same results as obtained from Eq. (24).

A pilot code was built to determine how well the above-described method worked for two-dimensional flow. The computed results agreed closely with those from other full-potential codes when the local Mach numbers remained subsonic, thus demonstrating that a panel method can be used to solve nonlinear problems if shocks are not present. However, the method proved to be unstable when supercritical flow cases were attempted.

Consequently, more powerful mathematical methods were pursued to solve nonlinear flow problems with shocks. One of these methods, which is related to the method just presented, is discussed in the next section.

III. Stable Panel/Rectangular-Grid Solution of Full-Potential Equation

Key Ideas

The method is iterative and each iteration requires solving two Poisson equations. The Poisson equations are obtained from the optimal control approach of Ref. 2. In Ref. 2, the Poisson equations are solved with the finite element method. In the current approach, the Poisson equations are solved with PAN AIR surface panels and the rectangular grid of points described earlier. The panels are used to enforce the boundary conditions, and the rectangular grid is used to evaluate the volume integral of Eq. (7) by fast Fourier transforms (FFTs). The grid is not used for the conventional purpose of replacing the governing partial differential equation [Eq. (1a)] with a system of finite difference equations. As will be seen in Sec. IV, the grid need not extend a large distance beyond the configuration. It needs only to extend to regions where the flow behaves linearly.

The mathematical development of the method is presented in Secs. 2.1, 3.0, and 4.0 of Ref. 6. Our purpose is to identify and, in a few instances, clarify the central steps of the method.

Linearization Step

The approximate mass flux vector $\vec{W}$ is defined to be

$$\vec{W} = \rho^* \vec{V} \tag{25}$$

where artificial (retarded) density ρ^* [see Ref. 6, Eq. (6)] is used in place of isentropic density. This is done so that only the physically relevant compression shock solutions are obtained. The approximate form of Eq. (1a) to be solved is then

$$\vec{\nabla}\cdot\vec{W} = 0 \tag{26}$$

An initial guess $\phi^{(1)}$ for the potential at each point of the rectangular grid will produce an error "e" at each grid point

$$e = \vec{\nabla}\cdot\vec{W}^{(1)} \tag{27}$$

To eliminate the error we need to find a change $\delta\phi$ in the potential such that the corresponding change in the mass flux vector $\delta\vec{W}$ gives

$$\vec{\nabla}\cdot\vec{W} = \vec{\nabla}\cdot\vec{W}^{(1)} + \vec{\nabla}\cdot\delta\vec{W} = 0 \tag{28}$$

The change $\delta\vec{W}$ is chosen to be the first term in the Taylor series,

$$\delta\vec{W} = \frac{\partial\vec{W}}{\partial u}\delta u + \frac{\partial\vec{W}}{\partial v}\delta v + \frac{\partial\vec{W}}{\partial w}\delta w \tag{29}$$

where u, v, and w are the components of $\vec{v} = \vec{\nabla}\phi$. The three partial derivatives in Eq. (28) can be expressed in terms of $\delta\vec{V}$ [see Ref. 6, Eq. (13)] and, hence, are computable from a change $\delta\phi$ where

$$\phi = \phi^{(1)} + \delta\phi \tag{30}$$

An iterative scheme for selecting $\delta\phi$ is needed so the resulting $\delta\vec{W}$ reduces the error e.

Scheme for Selecting $\delta\phi$

The optimal control approach of Ref. 2 is used to establish the criteria governing the selction of $\delta\phi$. First, for any trial function ϕ, numerically evaluate the divergence of $\vec{W}$. Second, introduce a state variable $\omega(x,y,z)$ defined everywhere by

$$\tilde{\nabla}^2\omega = -\alpha(x,y,z)\,\vec{\nabla}\cdot\vec{W} \tag{31a}$$

This state equation is the first of two (scaled) Poisson equations that will have to be solved. [The nonzero weighting function $\alpha(x,y,z)$ is introduced to provide faster convergence; optimal values can be determined from a von Neumann stability analysis. In the calculations made to date, $\alpha(x,y,z)$ has been set to unity. More will be said about this in the discussion of Fig. 7.]

As will be discussed later, in connection with the as yet undefined variable h_1, ω can be computed from

$$\omega(x,y,z) \equiv -\iiint_R \alpha(\vec{\nabla}\cdot\vec{W})K_o\,dR \tag{31b}$$

if boundary conditions exit only at infinity.

Third, define the scalar performance index J as follows [see Ref. 6, Eq. (9)]

$$J=\iiint_R\left[\left(\frac{1}{2}\right)\tilde{\nabla}\omega\cdot\vec{\nabla}\omega+\omega(\tilde{\nabla}^2\omega+\alpha\vec{\nabla}\cdot\vec{W})\right]dR \quad (32)$$

The first term in Eq. (32) is nonnegative for $M_\infty<1$, and the second term is zero because we are going to enforce Eq. (31a). Thus, J is nonnegative. The object is to find conditions on $\delta\phi$ that make δJ negative, and thus can be used to drive J to zero. When $J=0$, $\omega(x,y,z)$ is constant; hence $\tilde{\nabla}^2\omega$ is zero and $\vec{\nabla}\cdot\vec{W}=0$, as sought.

The calculus of variations is used to obtain δJ, and then three integrations by parts are performed to express δJ in terms of $\delta\phi$ and the other variables in the problem. The result is that δJ can be made negative if $\delta\phi$ is selected to be [see Ref. 6, Eq. (19)]

$$\delta\phi=\nu h, \qquad \nu>0 \text{ and const} \quad (33)$$

where $h(x,y,z)$ is the solution to a second Poisson equation

$$\tilde{\nabla}^2 h=p(\omega) \quad (34)$$

and where $p=-\vec{\nabla}\vec{F}$ is computable from ω and $\phi^{(1)}$ [see Eqs. (14) and (17) of Ref. 6] [$\vec{F}$ is defined following Eq. (14) of Ref. 6]. The integrations by parts also produce relationships that must be satisfied on the surface S, that is, the boundary conditions associated with h and ω. The boundary condition on h is

$$\hat{n}\cdot\tilde{\nabla}h=-\hat{n}\cdot\vec{F} \quad (35)$$

Thus, the problem of selecting $\delta\phi$ has led to the problem of solving two Poisson equations. First, Eq. (31a), subject to its boundary conditions [given prior to Eq. (13) of Ref. 6], must be solved to determine $\omega(x,y,z)$. Once $\omega(x,y,z)$ is determined, the right-hand side of Eq. (34) can be computed. Then Eq. (34) must be solved to determine $h(x,y,z)$, subject to boundary-condition equation (35). Finally, $\delta\phi$ is computed from Eq. (33).

Solving Poisson's Equation

The solution to either of the two Poisson equations is obtained by solving two simpler problems. For example, to solve Eq. (34), subject to Eq. (35), we solve the following:

Problem 1:

Partial differential equation $\tilde{\nabla}^2 h_1=p(\omega) \quad \omega=\omega(x,y,z)$

Boundary condition None‡ (36)

for $h_1(x,y,z)$ and then solve

Problem 2:

Partial differential equation $\tilde{\nabla}h_2=0$

Boundary condition $\hat{n}\cdot\tilde{\nabla}h_2=-\hat{n}\cdot\vec{F}-\hat{n}\cdot\tilde{\nabla}h_1$ on S (37)

for $h_2(x,y,z)$. The solution to Eq. (34), subject to Eq. (35), is then simply

$$h=h_1+h_2 \quad (38)$$

Equations (38), (37), and (36) correspond to Eqs. (2), (3), and (4), respectively, of Ref. 6. The solution to problem 1 is continuous everywhere, as if the aircraft surface were not present. The solution from problem 2 is discontinuous across the aircraft surface panels and acts like a boundary correction.

The solution to problem 1, for h at any point P, is

$$h_{1_P}\equiv\iiint_R p(x,y,z)K_\sigma dR \quad (39)$$

This is Green's third identity again [Eqs. (6) and (7)] for the situation in which there are no sources or doublets at the surface S.

Recall that K_σ depends on the difference between the fixed point P and the dummy integration point Q [see Eq. (5)]. This circumstance gives Eq. (39) an important property. The continuous Fourier transform of Eq. (39) changes the right-hand side from an integral of products (of physical variables) to just a product (of Fourier transforms). Thus, the integration problem in physical space becomes simply a multiplication problem in the transformed space. The continuous Fourier transform limits extend to plus and minus infinity. But, $\tilde{\nabla}^2 h_1$ turns out to be zero at points in physical space where nonlinear fluid-flow effects are negligible; this enables Eq. (39) to be written with finite limits. Hockney's mesh-doubling technique[14] is then used to treat the right-hand side of Eq. (39) as a periodic integral. This allows the volume integral of Eq. (39) to be evaluated with the highly efficient discrete§ FFTs instead of with continuous Fourier transforms.

The above approach has been coded and tested for a two-dimensional rectangular grid. The two-dimensional results indicate that in the three-dimensional case h_{1_p} can be computed at all points of a $128\times128\times128$ grid in less than 2 s of CPU time on a CRAY 1-S computer.

The solution to problem 2 is obtained with PAN AIR source and doublet panels. This can be done since Eq. (37) is of the same form as the Prandtl-Glauert equation.

Iteration Scheme

The overall iteration scheme is shown in Fig. 2. At the start of the outer (relinearization) loop, an initial guess is made for ϕ_i, the perturbation potential at each rectangular grid point "i." Dropping through to the inner (Poisson) loop, an initial guess is made for $\delta\phi_i$. This enables h_i to be computed at grid points and control points, and hence $\delta\phi_i$ is updated [Eq. (33)].

After several passes through the inner loop (although one pass seems to be sufficient in practice) the last set of values for $\delta\phi_i$ is used to update ϕ_i at the start of the outer loop. The process is repeated until the solution has converged, at which time $\tilde{\nabla}^2\omega=\vec{\nabla}\cdot\vec{W}=0$.

The problem 1 and 2 equations are solved during each pass through the inner (Poisson) loop. The PAN AIR solution to problem 2 leads to the equation

$$[\text{AIC}]\{\lambda\}=\{b\} \quad (40)$$

Recall from the right-hand side of Eq. (19) that $\{b\}$ is due to the boundary conditions. As seen from the second of Eqs. (37), the values in the boundary condition depend on h_1 (the solution to problem 1) and change with each iteration.

‡Although there are no boundary conditions of h_1 (or ω_1) at the aircraft surface S, h_1 (or ω_1) must be constant at infinity. This property occurs automatically because of the $1/r$ nature of K_σ, causing h_1 (or ω_1) to be zero at $r=\infty$.

§To use discrete Fourier transforms, the integrand of Eq. (30) must be continuous. Although the p term of the integrand is discontinuous across the panels, it is possible to remove this discontinuity without affecting the value of the definite integral. This is explained prior to Eq. (53) of Ref. 6.

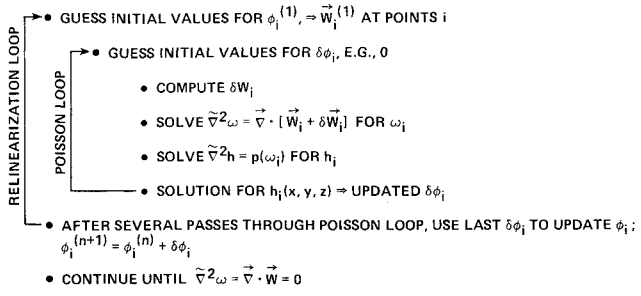

Fig. 2 Iteration scheme for method of Sec. III.

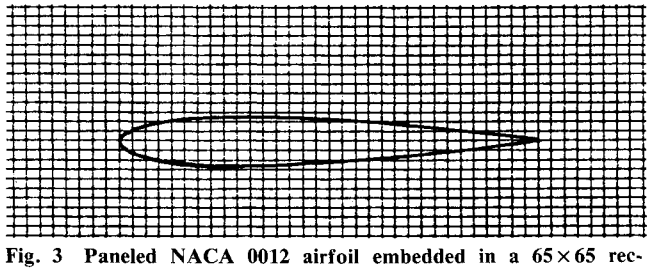

Fig. 3 Paneled NACA 0012 airfoil embedded in a 65×65 rectangular grid.

However, the AIC matrix does not change; it and its triangular decomposition need to be computed only once.

Also, the influence coefficients in the [AIC] matrix of Eq. (40) are only those that give the effects of the panels on the panel control points. To avoid computing influence coefficients for all of the grid points, the $\{\lambda\}$ determined from Eq. (40) is used to compute grid-point values of h_2 only at grid points near the panels. These values are then used in the right-hand side of Eq. (39), with h_2 replacing h_1, to compute h_2 at the not-near grid points. This process of spreading the effects of the panels to the grid is similar to what was done in the step 2, 3, 4 sequence in Sec. II.

IV. Results

Numerical results for two-dimensional flow are computed with a transonic PAN AIR research code that implements the method described in Sec. III.

NACA 0012 Airfoil

An NACA airfoil embedded in a rectangular grid of points is shown in Fig. 3. The airfoil surface is defined by 70 panels on each symmetric half. The actual NACA 0012 blunt trailing edge has been extended to 100.89% chord and forms a sharp trailing edge. In this figure, the grid of 65×65 points extends one-half chord upstream and downstream of the airfoil, and three-quarters of a chord above and below the airfoil.

The chordwise pressure coefficient distribution for this model, at a freestream Mach number of 0.80 and an angle of attack of 0 deg, is shown by the dashed curve of Fig. 4a. Increasing the number of grid points in the chordwise direction

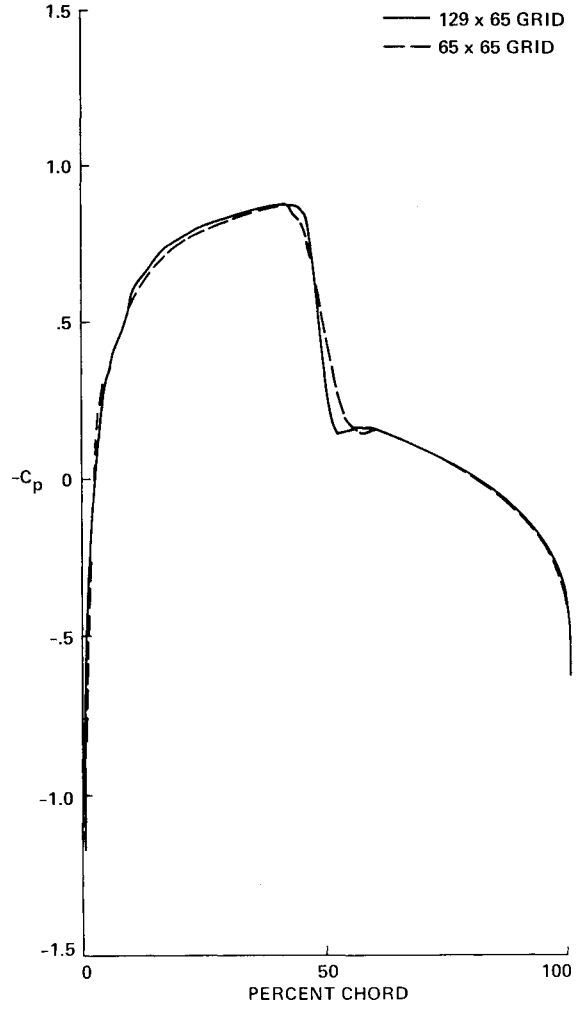

(a) CHORDWISE VARIATION IN C_p FOR 65 x 65 AND 129 x 65 RECTANGULAR GRID

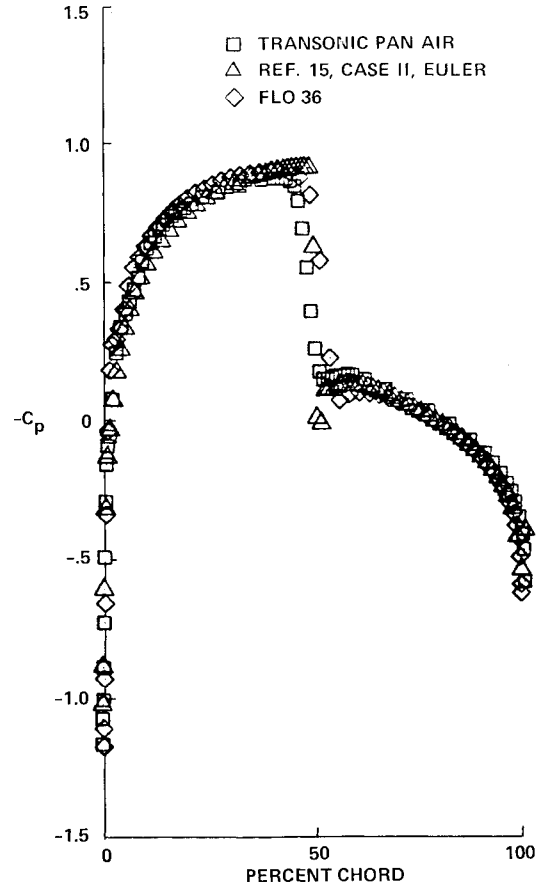

b) COMPARISON OF 129 × 65 PAN AIR RESULTS WITH SOLUTIONS FROM OTHER CODES

Fig. 4 Transonic PAN AIR results for nonlifting NACA 0012 airfoil: $M_\infty = 0.80$, $\alpha = 0$ deg, 70 panels on each half of airfoil.

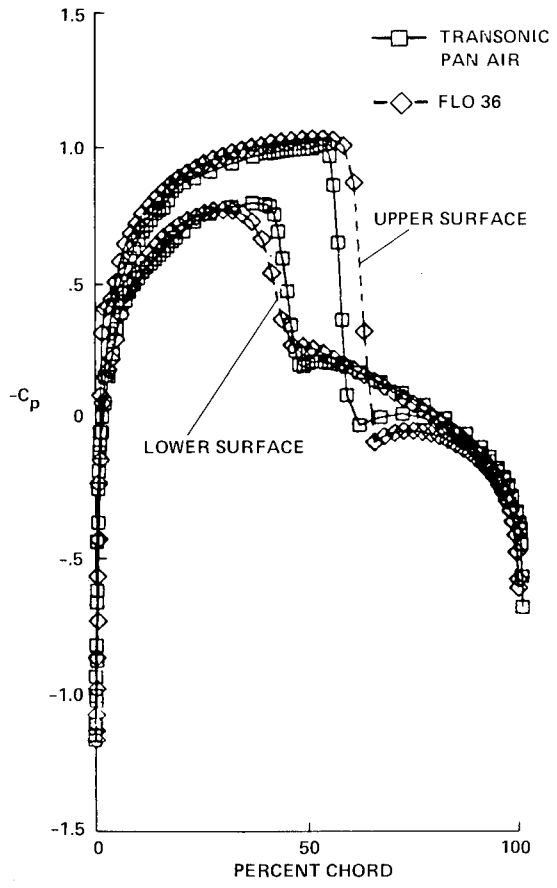

Fig. 5 Chordwise variation in C_p for supercritical flow about lifting NACA 0012 airfol; $M_\infty = 0.80$, $\alpha = 0.37$ deg.

to 129 produces the results given by the solid curve. The 129×65 grid predicts a slightly sharper shock than the 65×65 grid. Both solutions shown in Fig. 4a are converged to within plotting accuracy. The 129×65 grid solution required a little less than 901 iterations; the 65×65 grid solution required less than 501 iterations. The 129×65 grid solution (2700 s, CRAY 1-S) is also shown in Fig. 4b, along with a 128×32 mesh full-potential (conservative form) solution from the FLO-37 code (≈ 30 s, CRAY 1-S), and the 181×33 mesh Euler solution of Pulliam [Ref. 15, case II (625 s, CDC 7600)].

Supercritical lifting results for the NACA 0012 airfoil are shown in Fig. 5. Here, the freestream Mach number is 0.80 and the angle of attack is 0.37 deg. The solid curves through the square symbols are from the transonic PAN AIR code. A 129×65 grid was used that extended one-half chord ahead and behind the airfoil and a full chord above and below the airfoil. Comparison results, given by the dashed curves through the diamond symbols, are from FLO-36, again using a 128×32 mesh.

Circular-Arc Airfoil

There are no mesh coordinate transformations involved with the transonic PAN AIR method. Consequently, there are no problems when modeling airfoils with sharp leading edges, for example, a circular-arc airfoil. The leading-edge region, like the rest of the airfoil, is simply defined with panels.

Supercritical flow results for a nonlifting, 18%-thick, circular-arc airfoil are shown in Fig. 6. The solid curve is from the transonic PAN AIR code using a 129×65 rectangular grid (260 s, CRAY 1-S). The dashed curve is a comparison solution from the full potential code TAIR, using the consistent spatial-differencing scheme No. 3 of Ref. 16 (1.8 s, CRAY X-MP).

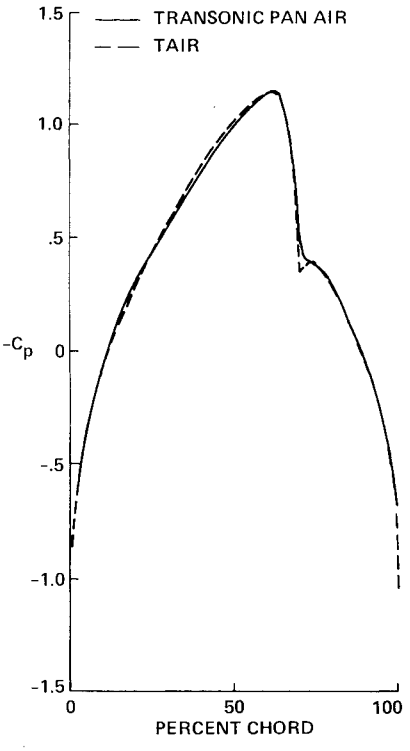

Fig. 6 C_p distribution of 18% thick circular-arc airfoil; $M_\infty = 0.73$, $\alpha = 0$ deg, 129×65 rectangular grid, 50 panels on each half of airfoil.

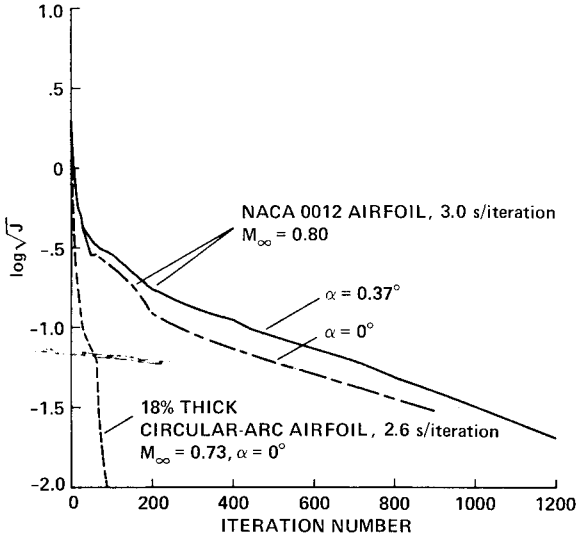

Fig. 7 Convergence behavior for transonic PAN AIR cases, 129×65 rectangular grid.

Convergence Behavior

A measure of the error at any given iteration is given by J of Eq. (32). The variation in the log of the square root of J with iteration number is presented in Fig. 7. For the two nonlifting cases, the circular-arc airfoil solution converges much more rapidly than that of the NACA 0012. The solution for a nonlifting NACA 0012 airfoil converges a little more rapidly than for the lifting case.

The slow convergence rate of the NACA 0012 is apparently due to the value 1.0 used for the scaling function $\alpha(x,y,z)$ in Eq. (31). With $\alpha(x,y,z) = 1.0$, values for h [from Eq. (38)] are quite large near blunt leading-edge stagnation points. This causes unreasonably large values of $\delta\phi = \nu h$ [Eq. (33)] near the stagnation point. Consequently, the constant step-size factor ν must be made smaller. This cures the leading-edge solution behavior, but also increases the number of iterations required since $\delta\phi$ is now smaller

everywhere. It should be possible to eliminate this problem by using a variable $\alpha(x,y,z)$.

V. Summary

A theoretical basis for extending panel methods to transonic flow has been presented. The approach uses surface singularity panels in combination with a rectangular set of grid points to predict transonic flow with shocks. The method has been demonstrated in two dimensions. Since the grid is rectangular in physical space, the entire problem of generating surface-conforming grids is avoided. Thus, extension to three dimensions appears practical if run times can be reduced significantly.

Acknowledgments

Bill Van Dalsem of NASA Ames computed the TAIR circular-arc airfoil results of Fig. 6. The research code used to compute the transonic PAN AIR results was written by the Boeing Company under a NASA Ames contract.

References

[1]Holst, T. L., Slooff, J. W., Yoshihara, H., and Ballhaus, W. F. Jr., "Applied Computational Transonic Aerodynamics," edited by B. M. Spee and H. Yoshihara, AGARD-AG-266, 1982, p. 86.

[2]Bristeau, M. O., Pironneau, O., Glowinski, R., Periaux, J., Perrier, P., and Poirier, G., "Application of Optimal Control and Finite Element Methods to the Calculation of Transonic Flows and Incompressible Viscous Flows," *Numerical Methods in Applied Fluid Dynamics*, edited by B. Hunt, Academic Press, New York 1980, pp. 203-312.

[3]Piers, W. J. and Slooff, J. W., "Calculation of Transonic Flow by Means of a Shock-Capturing Field Panel Method," AIAA Paper 79-1459, 1979.

[4]Tseng, K. and Morino, L., "Nonlinear Green's Function Method for Unsteady Transonic Flows," *AIAA Progress in Astronautics and Aeronautics, Transonic Aerodynamics*, Vol. 81, edited by D. Nixon, AIAA, New York, 1982, pp. 565-603.

[5]Oskam, B., "Transonic Panel Method for the Full Potential Equation Applied to Multi-Component Airfoils," AIAA Paper 83-1855, 1983.

[6]Johnson, F. T., James, R. M., Bussoletti, J. E., Woo, A. D., and Young, D. P., "A Transonic Rectangular Grid Embedded Panel Method," AIAA Paper 82-0953, 1982.

[7]Carmichael, R. L. and Erickson, L. L., "PAN AIR—A Higher Order Panel Method for Predicting Subsonic or Supersonic Linear Potential Flows about Arbitrary Configurations," AIAA Paper 81-1255, 1981.

[8]Derbyshire, T. and Sidwell, K. W., "PAN AIR Summary Document (Version 1.0)," NASA CR-3250, 1982.

[9]"PAN AIR—A Computer Program for Predicting Subsonic or Supersonic Linear Potential Flows about Arbitrary Configurations Using a Higher Order Panel Method (Version 1.0). Vol. I. Theory Document," NASA CR-3251, 1980.

[10]Erickson, L. L. and Strande, S. M., "PAN AIR: Evolution and New Directions...Transonics for Arbitrary Configurations," AIAA Paper 83-1831, 1983.

[11]Jameson, A., "Transonic Flow Calculations," *Numerical Methods in Fluid Dynamics*, edited by H. J. Wirz and J. J. Smolderen, McGraw-Hill Book Co., New York, 1978.

[12]Liepmann, H. W. and Roshko, A., *Elements of Gasdynamics*, John Wiley and Sons, New York, 1957.

[13]Kellogg, O. D., *Foundations of Potential Theory*, Dover Publications, New York, 1954.

[14]Hockney, R. W., "The Potential Calculation and Some Applications," *Methods in Computational Physics*, Vol. 9, Academic Press, New York, 1969.

[15]Pulliam, T. H., Jespersen, D. C., and Childs, R. E., "An Enhanced Version of an Implicit Code for the Euler Equations," AIAA Paper 83-0344, 1983.

[16]Flores, J., Holst, T. L., Kwak, D., and Batiste, D. M., "A New Consistent Spatial Differencing Scheme for the Transonic Full-Potential Equation," AIAA Paper 83-0539, 1983.

[17]Johnson, F. T., private communication, Boeing Co., Seattle, WA, June 1983.